

Fractals in rate-induced tipping

Jason Qianchuan Wang,^{1, a)} Yi Zheng,^{1, a)} and Eduardo G. Altmann¹

School of Mathematics and Statistics, The University of Sydney, Sydney, Australia

(*Electronic mail: eduardo.altmann@sydney.edu.au)

(Dated: 26 January 2026)

When parameters of a dynamical system change sufficiently fast, critical transitions can take place even in the absence of bifurcations. This phenomenon is known as rate-induced tipping and has been reported in a variety of systems, from simple ordinary differential equations and maps to mathematical models in climate sciences and ecology. In most examples, the transition happens at a critical rate of parameter change, a rate-induced tipping point, and is associated with a simple unstable orbit (edge state). In this work, we show how this simple picture changes when non-attracting fractal sets exist in the autonomous system, a ubiquitous situation in non-linear dynamics. We show that these fractals in phase space induce fractals in parameter space, which control the rates and parameter changes that result in tipping. We explain how such rate-induced fractals appear and how the fractal dimensions of the different sets are related to each other. We illustrate our general theory in three paradigmatic systems: a piecewise linear one-dimensional map, the two-dimensional Hénon map, and a forced pendulum.

I. INTRODUCTION

Tipping points in climate and ecological models have renewed the interest in understanding dynamical processes leading to sudden changes in otherwise stable states^{1–4}. Rate-induced tipping (R-tipping)¹ is a mechanism leading to such change in non-autonomous dynamical systems with time-dependent parameters, as observed and studied in a variety of systems in the last two decades^{1–11}. In R-tipping, the dynamics *tracks* the same stable state if parameters change slowly (small rate r), but *tips* out of it if the change is fast (large rate r). The tipping point is associated with a critical rate (r_c). In the simplest and paradigmatic examples of R-tipping, this critical rate is at the tracking-tipping boundary and leads to trajectories approaching an *edge state* that is an unstable fixed point^{1,7} or periodic orbit^{5,8} of the autonomous dynamics.

R-tipping is an example of the important role played by unstable orbits in non-linear systems, even if these orbits are not directly observed. Similarly, in the study of *transient chaos*^{12–14}, fractal invariant saddles are the central object of interest, as they control the most relevant dynamical and observable quantities: the escape rate of the saddle controls the rate in which trajectories escape or transition between attractors; the stable manifold of the saddle often acts as a fractal basin boundary between attractors or escape directions; and the fractal dimension of the saddle can be connected to both the escape rate and the Lyapunov exponent of the transient chaotic dynamics. Importantly, such fractal sets appear in many different non-linear dynamical systems without the need of fine-tuning of parameters, as illustrated by the wide range of examples reviewed in the literature^{12–14}.

In this paper, we investigate the effect of fractal saddles on R-tipping. We show how these saddles, together with the transient chaotic dynamics they induce, create extreme sensitivity of the dependence of the tracking and tipping asymptotic states on how parameters change. We discuss the conditions under which the fractal dimension of the boundary

between these states can be connected to the fractal dimension of the saddles, and how they can be connected to each other. Our study is inspired by, and intends to contribute to, recent extensions of the applicability of R-tipping: Refs. 6,11,15 considered different interplays between chaotic dynamics and tipping; Refs. 3,10,16 reported the appearance of fractal and chaotic edge states in climate models; and Refs. 4,8 pointed to the importance of investigating the effect of fractal saddles on R-tipping.

The paper is divided as follows. We start in Sec. II with the definitions and mathematical formalism for the study of R-tipping in (discrete-time) dynamical systems⁷. In Sec. III, we investigate examples of dynamical systems showing fractal R-tipping, including numerical evidence of the equality of the fractal co-dimension of the three different sets. This motivates the introduction, in Sec. IV, of a general mechanism that explains the numerical observations. Finally, we conclude and discuss our results in Sec. V. Detailed derivations and numerical simulations of additional cases are reported in the Appendices and the code to re-produce our results is available in our repository¹⁷.

II. GENERAL FORMALISM

Here we investigate generic R-tipping phenomena following the discrete-time formalism introduced in Ref.⁷. The autonomous dynamics is defined by a \mathbb{C}^0 (continuous) function F with parameters $\lambda \in \mathbb{R}^m$ that maps points $x \in \Omega$ from and to the phase space $\Omega \subseteq \mathbb{R}^d$ as

$$x_{n+1} = F(x_n; \lambda), \quad (1)$$

where $n \in \mathbb{Z}$ is the discrete time. The non-autonomous dynamics is obtained by changing the parameters λ in time as

$$\begin{aligned} x_{n+1} &= F(x_n; \Lambda(s_n)), \\ s_n &= rn. \end{aligned} \quad (2)$$

where $r \geq 0$ is the *rate* of change of λ and $\Lambda(s) = \Lambda(s_n)$ is the protocol specifying the path of parameter change, which

^{a)}These authors contributed equally to this work.

we consider a \mathbb{C}^0 (continuous) function $\mathbb{R} \mapsto \mathbb{R}^m$. We will consider different paths $\Lambda(s)$ such that $\lambda_0 = \Lambda(s=0)$ (at $n=0$) and

$$\lambda_{\pm} = \lim_{s \rightarrow \pm\infty} \Lambda(s). \quad (3)$$

We consider autonomous dynamical systems F that show multi-stability, i.e., for which different initial conditions in Eq. (1) lead to more than one asymptotic ($n \rightarrow \infty$) state (e.g., attractors). For simplicity, in the examples we consider below one of such asymptotic states is a stable fixed point $x^*(\lambda)$ and we study whether trajectories starting at $x^*(\lambda)$ track or tip from $x^*(\lambda)$ as the parameter λ changes according to $\Lambda(s)$. As we are interested exclusively in R-tipping, rather than in tipping due to bifurcations, we focus on parameter changes that follow a *stable paths*, i.e., parameter paths $\Lambda(s)$ so that $x^*(\lambda)$ is stable for all $\lambda \in \Lambda(s)$. As to initial conditions x_0 , we primarily consider trajectories starting at the fixed point $x^*(\Lambda(s))$, either at $s = n = 0$ or at $s \rightarrow -\infty$, depending on the choice of $\Lambda(s)$. If asymptotically the trajectory approaches the stable fixed point $x^*(\lambda_+)$ of the frozen system $F(x, \lambda_+)$, we say that it *tracks*. Otherwise, we say that it *tips* (e.g., if the trajectory approaches another attractor of $F(x, \lambda_+)$ or diverges). We thus define the tipping function ϕ as

$$\phi(r, x_0; \Lambda(s)) = \begin{cases} \text{track} & \text{if } \lim_{n \rightarrow \infty} x(n) = x^*(\lambda_+), \\ \text{tip} & \text{otherwise,} \end{cases} \quad (4)$$

where $x(n)$ is obtained by iterating Eq. (2). Contrary to alternative definitions^{4,8}, ϕ in Eq. (4) considers only the $n \rightarrow \infty$ behaviour of x and classifies as tracking the trajectories that depart the vicinity of $x^*(\lambda(n))$ but that eventually settle into it. We will characterize R-tipping due to basin crossing²⁻⁴ by identifying variations of r , x_0 , and $\Lambda(s)$ that lead to a change in the outcome of ϕ . The parameter values at which this happens will be denoted critical or boundary values. with initial condition $x^*(\Lambda(s))$ (at $s = 0$ or $s \rightarrow -\infty$ depending on $\Lambda(s)$).

Since the parameters λ are changing in a stable path $\Lambda(s)$ and the initial condition is in x^* , for sufficiently small rate r the trajectory tracks⁷. As the rate of parameter change r grows, the trajectory *may tip*. A rate $r = r_c$ is called critical if it is at the boundary between tracking and tipping, i.e., if every open interval around r_c contains both $\phi = \text{track}$ and $\phi = \text{tip}$. In particular, we denote the smallest critical r as r_{c1} . In the traditional (simplest) examples of R-tipping, there is only one such point r_c (tipping point), and it is associated with an unstable fixed point – an *edge state* – that is approached when $r = r_c$. In order to observe fractals in R-tipping, the key idea we follow^{3,4,8} is to explore the consequence of fractal saddles acting as edge states to the transition between tracking and tipping, as quantified by the dependence of the tipping function $\phi(r, x_0; \Lambda(s))$ – defined in Eq. (4) – on the tipping related parameter r and the path $\Lambda(s)$.

III. EXAMPLES

We now investigate the effect of fractal saddles in R-tipping using three simple maps F_A , F_B , and F_C as F in Eq. (2).

A. Piecewise-linear map ($d = 1$)

We start by constructing a simple example of dynamical system showing fractal R-tipping. Our starting point is the open tent map

$$x_{n+1} = \begin{cases} \mu x_n, & x_n < 1/2, \\ \mu (1 - x_n), & x_n \geq 1/2, \end{cases} \quad (5)$$

where $x \in \mathbb{R}$ and $\mu \geq 2$ is a parameter. For $\mu = 2$, the closed tent map is recovered, which leads to a fully chaotic dynamics in $x \in [0, 1]$. For $\mu > 2$, with probability one, randomly selected initial conditions $x_0 \in [0, 1]$ diverge to $-\infty$ as $n \rightarrow \infty$. Nevertheless, there is a Lebesgue measure zero set of non-escaping points that build a fractal repeller. For $\mu = 3$, which we use throughout this paper, the repeller is the middle-third Cantor set¹³.

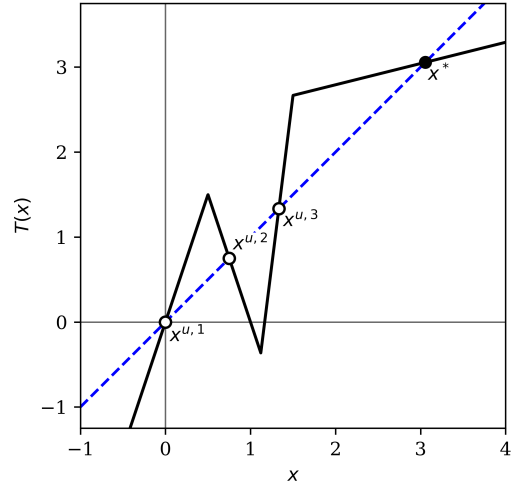
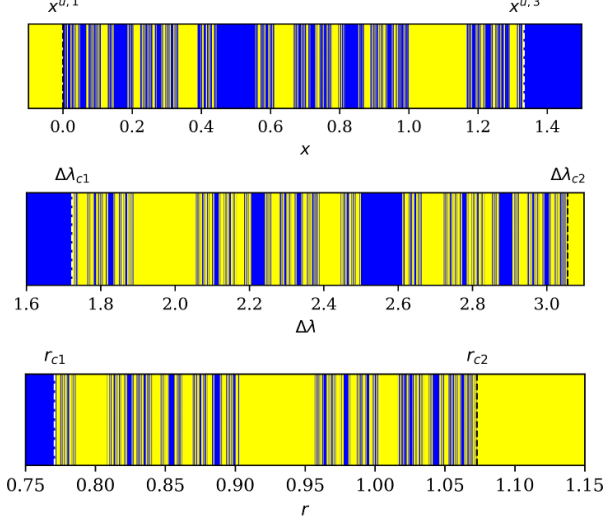


FIG. 1: Graphical representation of the modified tent map $T(x)$ in Eq. (6). There are four fixed points at the intersection of $T(x)$ (solid line) and the diagonal $y = x$ (dashed blue line): two unstable as in the open tent map ($x^{u,1} = 0$ and $x^{u,2} = 3/4$), a third unstable ($x^{u,3} = 4/3$) in the intermediate interval ($37/33 < x < 3/2$), and one stable ($x^* = 55/18$). We investigate R-tipping out of x^* by shifting this map along the diagonal – see Eqs. (7)-(8).

We now modify the tent map in Eq. (5) to obtain a new map $T(x)$ in which R-tipping can take place. To introduce multi-stability, we require T to have a fixed point $x^* = T(x^*)$ that is stable ($|T'(x^*)| < 1$) and on the right of the domain of the tent map, i.e., $x^* > 1$. A simple modification of Eq. (5) that achieves this, retaining $T(x)$ as a piecewise linear continuous

(a)



(b)

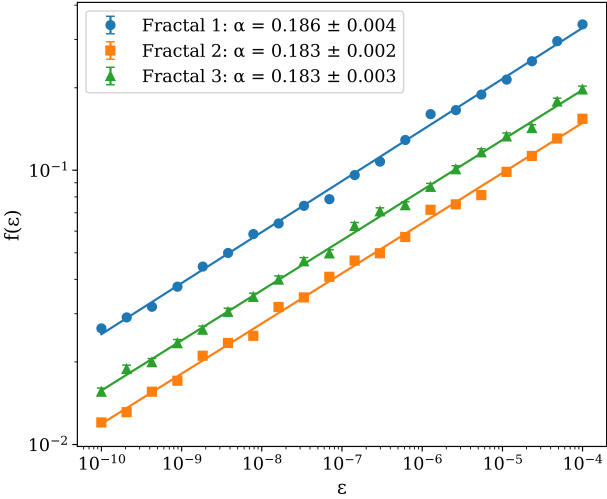


FIG. 2: The three fractals in the piecewise-linear map (7) have the same co-dimension α . (a) Plot of the function $\phi(r, x_0; \Lambda(s))$ in Eq. (4) – with blue corresponding to $\phi = \text{track}$ and yellow to $\phi = \text{tip}$ – as a function of different parameters (top to bottom): initial conditions $x = x_0$ (with $r = \lambda_+ = 0$, Fractal 1); range of parameter variation $\Delta\lambda = 2\lambda_+$ used in $\Lambda(s)$ (with $r \rightarrow \infty$, Fractal 2); and rate of change r (with $\Delta\lambda = 4$, Fractal 3). (b) Estimation of the fractal co-dimension α of the track/tip boundary for the three fractals shown in panel (a). We use the uncertainty algorithm^{12,18} to estimate α as the slope of the scaling between the fraction of ε -uncertain points $f(\varepsilon)$ and ε ; see Appendix C for details. Data for Fractal 1 is multiplied by 2 for clarity.

function and using $\mu = 3$, is to add two new branches as

$$x_{n+1} = T(x_n) = \begin{cases} 3x_n, & x_n < 1/2 \\ 3(1-x_n), & 1/2 \leq x_n < \frac{37}{33} \\ 8x_n - \frac{28}{3}, & \frac{37}{33} \leq x_n < \frac{3}{2}, \\ \frac{1}{4}x_n + \frac{55}{24}, & x_n \geq \frac{3}{2}. \end{cases} \quad (6)$$

This function is plotted in Fig. 1. Initial conditions in the last branch ($x \geq 3/2$) converge to the stable fixed point ($x^* = 55/18 = 3.0\bar{5}$) due to the choice of its slope $T'(x^*) = 1/4 < 1$. The remaining parameters of the two branches were chosen in such a way that the interval $x \in [1, 3/2]$ is split in three equal sized sub-intervals such that $x \in [1, 7/6]$ leads immediately to escape (i.e., $T(x) < 0 \Rightarrow x \rightarrow -\infty$), $x \in [7/6, 4/3]$ leads to a re-injection in the tent map domain (i.e., $T(x) \in [0, 1]$), and $x \in [4/3, 3/2]$ leads to the stable fixed point (i.e., $x \rightarrow x^*$).

We now consider non-autonomous changes of the map (6) that can induce R-tipping out of the stable fixed point x^* . As in Ref.⁷ (Example 4.2), we introduce a new map F_A with a parameter λ that preserves the dynamics and simply shifts $T(x)$ along the line $y = x$ as

$$x_{n+1} = F_A(x_n; \lambda) = T(x_n - \lambda) + \lambda, \quad (7)$$

with T given by Eq. (6), see Appendix A for an explicit expression of F_A for arbitrary parameters. In particular, the four fixed points of $T(x)$ appear as fixed points of $F_A(x)$ shifted by λ , i.e., $x^* + \lambda$ is a stable and $x^{u,i} + \lambda$ ($i = 1, 2, 3$) are unstable fixed points of $F_A(x, \lambda)$.

The map F_A is a $d = 1$ example of the map F in Eq. (2). The non-autonomous system (2) is obtained by specifying a protocol $\Lambda(s)$ for the parameter change, which here we use

$$\Lambda_A(s) = \lambda_+ \tanh(s) = \lambda_+ \tanh(rn), \quad (8)$$

and initial condition $x = x^*$ ($\lambda_- = -\lambda_+$) at $n \rightarrow -\infty$ so that the trajectory x_n corresponds to the pullback attractor of x^* as in Ref.⁷.

We now investigate R-tipping in the dynamical system (2) defined by Eqs. (6)-(8). We focus on the dependence of the tipping function ϕ in Eq. (4) on $\Delta\lambda = \lambda_+ - \lambda_- = 2\lambda_+$ and r in Eq. (8), which together uniquely specify the parameter change. For sufficiently small $r < r_{c1}$ and $\Delta\lambda < \Delta\lambda_{c1}$, $\phi = \text{track}$ because the parameter variation is in a stable path. The small $r, \Delta\lambda$ regime is valid up to the first critical values $\Delta\lambda_{c1} = 31/18$ and $r_{c1} \approx 0.771$, which can be computed considering the first time trajectories x_n cross the frozen path $(x^{u,3}(\Lambda(s)), s)$ of the largest unstable fixed point $x^{u,3}$. Similarly, for sufficient large $\Delta\lambda \geq \Delta\lambda_{c2} = 55/18$ and $r \geq r_{c2} \approx 1.073$, the trajectory crosses the frozen path of the smallest unstable fixed point $(x^{u,1}(\Lambda(s)), s)$ and therefore $\phi = \text{tip}$. We are also particularly interested in the case $\Delta\lambda$ for $r \rightarrow \infty$ because the appearance of $\phi = \text{tip}$ for any $\Delta\lambda$ in this case is a sufficient condition for the appearance of R-tipping⁷. Figure 2 shows numerical results of the dependence of ϕ on $x, \Delta\lambda$, and r . They confirm the prediction of track (tip) for parameters below (above) the first (second) critical value r_{c1} (r_{c2}). More interestingly, the numerical results show that in between these values, there is an intricate variation between $\phi = \text{track}$ and

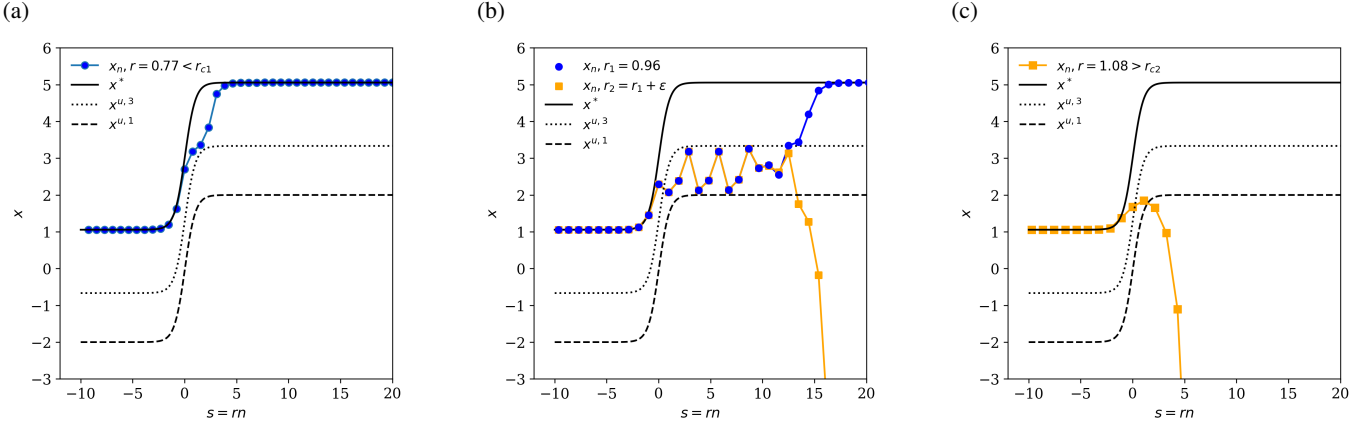


FIG. 3: Tracking and tipping trajectories in the non-autonomous piecewise-linear map defined by Eqs. (6)-(8). The three panels show the frozen paths of the stable – $(x^*(\Lambda(s)), s)$ as solid line – and unstable fixed points – $(x^{u,1}(\Lambda(s)), s)$ and $(x^{u,3}(\Lambda(s)), s)$ as dashed and dotted black lines, respectively –, and the trajectory x_n obtained starting at x^* for $n \rightarrow -\infty$ and evolving using Eq. (2) with $F = F_1$ – in Eq. (7) – and $\Lambda(s)$ – in Eq. (8) – with parameters $\lambda_+ = 2$ and different values of the rate r of parameter change: (a) small rate $r = 0.77 < r_{c1} \approx 0.7708$, leading to a tracking trajectory; (b) two similar rates $r_1 = 0.96243528753$ and $r_2 = r_1 + 10^{-9}$ close to a critical rate $r_{c1} < r_c < r_{c2}$ (boundary point), leading to both tracking and a tipping trajectories; and (c) large rate $r = 1.08 > r_{c2} \approx 1.0727$, leading to a tipping trajectory.

$\phi = \text{tip}$. The boundary between these two regimes is a fractal with a dimension equal to the dimension of the boundary obtained varying the initial condition x (for $r = \Delta\lambda = 0$, fractal repeller of the autonomous map) and $\Delta\lambda$ (for $r \rightarrow \infty$).

We now explain the connection between the three fractal observations reported above. The repeller of the autonomous map (6) (Fractal 1) is composed of the union of the middle third Cantor set of the tent map (5) and other components in $x \in [0, 4/3] \equiv [x^{u,1}, x^{u,3}]$ created by the third linear branch in Eq. (6) due to re-injection. This fractal can be directly connected to the fractal in $\Delta\lambda$ (for $r \rightarrow \infty$, Fractal 2) by noting that, due to the simplicity of the effect of λ in the dynamics specified in Eq. (7), a variation $\Delta\lambda$ is equivalent to the dynamics at λ_+ with the initial condition given by one map (6) iteration $F_A(x_0, \lambda = \lambda(s=0) = 0)$ of the initial condition $x_0 = x^*(\lambda = \lambda_- = -\lambda_+)$. The connection to the fractal in r (fixed $\Delta\lambda > \Delta\lambda_{c1}$, Fractal 3) to the other fractals is more subtle and will be fully discussed in the next section. An intuitive explanation is that for values $r_{c1} < r < r_{c2}$ the trajectories enter the region $x^{u,1} < x < x^{u,3}$ and experience a transiently chaotic dynamics. The closer r is to any critical rate r_c , the longer x_n spends between the (frozen path of the) unstable periodic orbits reproducing closely the dynamics of the fractal repeller (at $\lambda = \lambda_+$). This picture is confirmed in Fig. 3, which shows the dynamics of tracking and tipping trajectories for different r 's.

B. Hénon map ($d = 2$)

Our second example is chosen to show that the appearance of fractals in R-tipping does not require a carefully designed dynamical system. We thus consider one of the most-studied

simple systems with complex dynamics, the Hénon map

$$F_B = \begin{cases} x_{n+1} &= 1 - ax_n^2 + y_n, \\ y_{n+1} &= bx_n, \end{cases} \quad (9)$$

where $\lambda = (a, b) \in \mathbb{R}^2$ are parameters. Here we restrict our analysis to parameters in the set $\Gamma \subset \mathbb{R}^2$, with

$$\Gamma = \left\{ (a, b) : a \in \left(\frac{-(1-b)^2}{4}, \frac{3(1-b)^2}{4} \right), |b| < 1, a \neq 0 \right\}, \quad (10)$$

because for $\lambda \in \Gamma$ the point

$$(x^*, y^*) = \left(\frac{-(1-b) + \sqrt{(1-b)^2 + 4a}}{2a}, bx^* \right) \quad (11)$$

is a *stable* fixed point of Eq. (9). Figure 4 plots the set Γ (panel a) and the basin of attraction of the stable fixed point (x^*, y^*) (panel b) for two (pairs of) parameters $\lambda \in \Gamma$. The numerical results confirm that both smooth and fractal basin boundaries are observed, depending on the parameters¹⁹.

To observe R-tipping in the Hénon map using a stable path $\Lambda(s)$, we vary the parameter pair (a, b) from a starting pair $\lambda_0 = (a_0, b_0) \in \Gamma$ to an end pair $\lambda_+ = (a_+, b_+) \in \Gamma$. The simplest choice of path, which we will use in our analysis for finite r , is a linear path between these points parameterized by

$$\Lambda_B(s) = \begin{cases} \lambda_0 & \text{for } s < 0, \\ \lambda_0 + (\lambda_+ - \lambda_0) \tanh(s) & \text{for } s \geq 0, \end{cases} \quad (12)$$

where $\lambda = (a, b)$ and $s = rn$. In Eq. (12), we restrict the change to $s > 0$ (i.e., we take $\lambda_- = \lambda_0$) – contrary to the approach taken in the first example (8) – to illustrate the validity

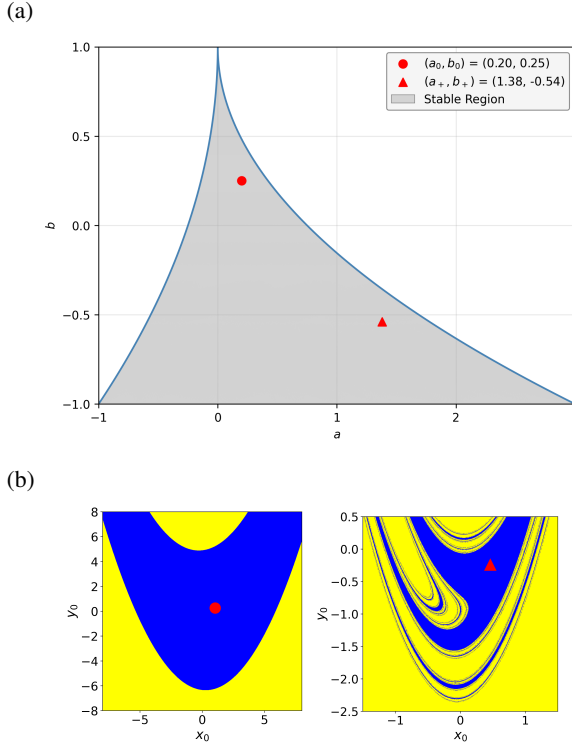


FIG. 4: The basin of attraction of the fixed point of the Hénon map can have smooth or fractal boundaries. (a) Parameter space $\lambda = (a, b)$ of the Hénon map (9). The gray shaded region corresponds to the region Γ for which the fixed point (11) is stable, defined in Eq. (10). The two highlighted points indicate the values $\lambda_0 = (a_0, b_0)$ and $\lambda_+ = (a_+, b_+)$ used in our investigation (see legend). (b) The basin of attraction (in blue) of the stable fixed point (red symbol) for $\lambda = \lambda_0$ (left, smooth boundary) and $\lambda = \lambda_+$ (right, fractal boundary).

of our results for different choices of paths $\Lambda(s)$ and to simplify the numerical calculations²⁰. Below we report numerical results of the tracking/tipping function (4) based on the dynamics (2) for the map $F = F_B$ in Eq. (9) with parameters evolving as in Eq. (12) and initial condition given by the fixed point (11) with $(a, b) = (a_0, b_0) \equiv \lambda_0$.

We start our investigation considering whether R-tipping takes place for a given choice of $\lambda_0 = (a_0, b_0)$ and $\lambda_+ = (a_+, b_+)$. Considering that λ changes in a stable parameter path inside Γ , we know that for sufficiently small r we have $\phi = \text{track}$. Therefore, a value of $\phi = \text{tip}$ for $r \rightarrow \infty$ implies that at least one $r_c > 0$ exists. Based on the results in Ref.⁷, a sufficient condition is thus to check whether the fixed point (11) with $\lambda = \lambda_0$ is in the basin of attraction of the fixed point with $\lambda = \lambda_+$. This can be done by fixing either λ_0 or λ_+ and exhaustively exploring Γ . Figure 5 shows the numerical results: fixing λ_0 , we obtain — Fig. 5(a) — a parameter space Γ with an intricate boundary between tracking and tipping, suggesting that smooth boundaries (on the bottom left) co-exist with fractal boundaries (bottom right); fixing λ_+ to a value in which the corresponding fixed point (x^*, y^*) has a fractal basin boundary

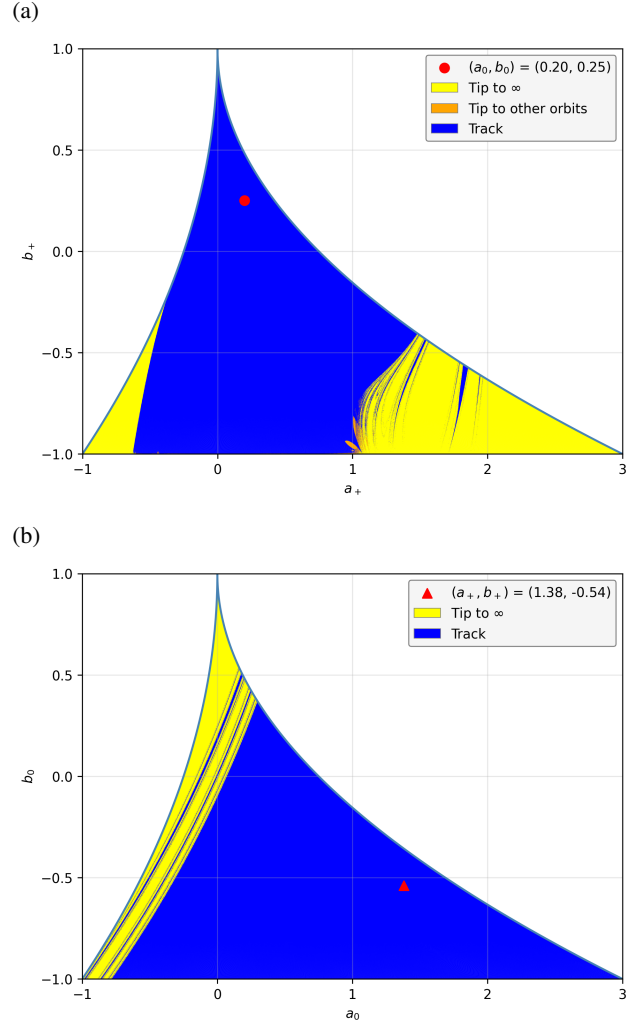


FIG. 5: Fractal boundary between tracking and tipping regions in the parameter space Γ of the Hénon map. Initial conditions at the fixed point $(x_0, y_0) = (x_0^*, y_0^*)$ of $\lambda_0 = (a_0, b_0)$ are iterated using Eq. (9) with $\lambda = \lambda_+ = (a_+, b_+)$. (a) Dependence of ϕ on (a_+, b_+) for a fixed $(a_0, b_0) = (0.20, 0.25)$. (b) Dependence of ϕ on (a_0, b_0) for a fixed $(a_+, b_+) = (1.38, -0.54)$. The fixed values of λ_0 and λ_+ (red symbols, see legend) are the same used in Fig. 4. Parameters λ_0 and λ_+ showing $\phi = \text{tip}$ will display R-tipping with at least one critical tipping rate r_c .

(Fig. 4(b), bottom right), we obtain — Fig. 5(b) — a separation of the parameter space Γ that suggests a fractal boundary with a dimension between 1 and 2 (i.e., co-dimension $0 < \alpha < 1$).

We now focus on quantifying the fractality of the tracking/tipping boundaries. We focus on three cases: the basin of attraction of the fixed point at λ_+ (Fractal 1, shown in Fig. 4(b), right); the parameter space Γ varying $\lambda_+ = (a_+, b_+)$ for $r \rightarrow \infty$ (Fractal 2, shown in Fig. 5(a)); and the dependence on the rate r for fixed λ_0 and λ_+ , in which cases the boundaries correspond to critical values r_c (Fractal 3). The numerical results are reported in Fig. 6 and strongly suggest that the

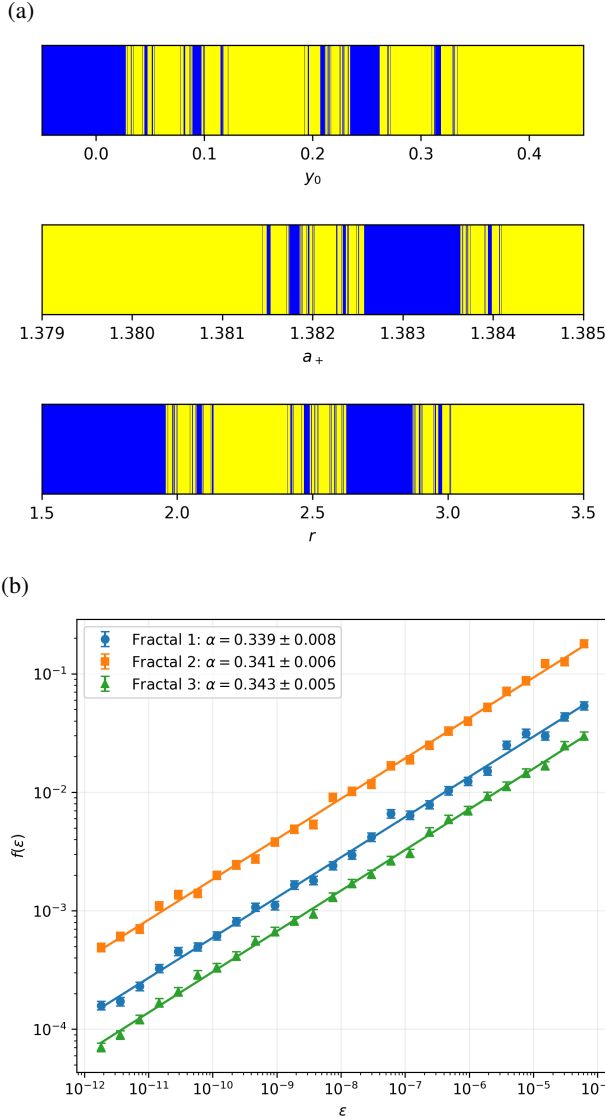


FIG. 6: The three fractals in the Hénon map (9) have the same co-dimension α . (a) Plot of $\phi(r, x_0; \Lambda(s))$ in Eq. (4) – with blue corresponding to $\phi = \text{track}$ and yellow to $\phi = \text{tip}$ – as a function of different parameters (top to bottom): initial conditions ($x_0 = -0.2, y_0$), corresponding to the basin-of-attraction of the fixed point for the end parameter (a_+, b_+) = (1.38, -0.54) (Fractal 1); the end parameter value (a_+, b_+ = -0.54), for a fixed starting parameter (a_0, b_0) = (0.20, 0.25) (Fractal 2); rate r using (a_0, b_0) = (0.20, 0.25) and (a_+, b_+) = (1.38, -0.54) (Fractal 3) under parameter path Eq. (12). (b) Estimation of the fractal co-dimension α of the track/tip boundary for the three fractals shown in panel (a) based on the uncertainty algorithm^{12,18}. We estimate α as the slope of the scaling between the fraction of ε -uncertain points $f(\varepsilon)$ and ε ; see Appendix C for details.

three boundaries are fractal with the same co-dimension α . In particular, Fractal 3 is computed choosing a value of λ_+ for which $\phi = \text{tip}$ when $r \rightarrow \infty$, which we argued above ensures

the existence of at least one critical r_c . In fact, our results suggest that there infinitely many r_c 's, distributed in a fractal set with dimension $D = 1 - \alpha \approx 0.657 \pm 0.005$. This is obtained for a path $\Lambda(s)$ which finishes at a parameter $\lambda_+ = (a_+, b_+)$ for which x^* has a fractal basin boundary. Instead, if a λ_+ with a smooth boundary is chosen (see Figs. 4-5), a smooth transition in the ϕ dependence on λ_+ and r are observed, as shown in Appendix B.

C. Forced Pendulum

Our third example is a physical system: the continuous-time t dynamics of a damped forced pendulum¹⁹, defined by the second order differential equation

$$\ddot{\theta} + 0.1\dot{\theta} + \sin(\theta) = \lambda \cos(t), \quad (13)$$

where $\theta \in [0, 2\pi]$ is the angle position of the pendulum, $\dot{\theta} \equiv d\theta/dt$ is the angular velocity, and λ is the intensity of the forcing (the only free parameter). The other physical parameters are fixed: damping strength to 0.1 and both the natural and forcing frequencies to 1. We use a Poincaré surface of section obtained every period 2π of the forcing, i.e., for $t = 2\pi n$ with $n \in \mathbb{Z}$, which induces a discrete-time map F_C – as in Eq. (1) – that maps $(\dot{\theta}, \theta)_n$ to $(\dot{\theta}, \theta)_{n+1}$. In practice, F_3 is computed by integrating numerically Eq. (13)¹⁷. For sufficiently small forcing strength λ , the oscillation with period one is a stable periodic orbit of the flow and thus a stable fixed point $x^* = (\dot{\theta}^*, \theta^*)$ of the map F_C . As investigated in the seminal paper¹⁹, at values $\lambda \gtrsim 1$ the basin of attraction of this fixed point has a fractal boundary.

Here we use this paradigmatic example of fractal basin-boundary to test the R-tipping fractal phenomenology observed in the previous examples. As the parameter-change protocol, we use a linear ramp from $\lambda = 0$ to $\lambda = \lambda_+$ as

$$\Lambda_C(s) = \begin{cases} 0 & \text{for } s < 0, \\ s & \text{for } 0 \leq s \leq \lambda_+, \\ \lambda_+ & \text{for } s > \lambda_+, \end{cases} \quad (14)$$

with $\lambda_+ = 1.195$ (in which a fractal basin boundary is present) and $s = rt$ in continuous time t , i.e., $\dot{s} = t$, which is different from the discrete-time definition in Eq. (2) but more natural when modeling the variable forcing of a pendulum. The numerical results reported in Fig. 7 show a fractal dependence on the tipping parameters λ_+ and r with the same fractal dimension of the basin boundary, confirming the observations obtained in the two previous examples.

IV. THEORETICAL INTERPRETATION

The numerical experiments above show that, in all three examples, fractals appear in the dependence of the tipping function ϕ on the rate r and amplitude $\Delta\lambda$ (or λ_+) of parameter change. More precisely, the infinitely many values in which ϕ changes outcome are fractally distributed with a fractal co-dimension that is equal to the co-dimension of the fractal basin

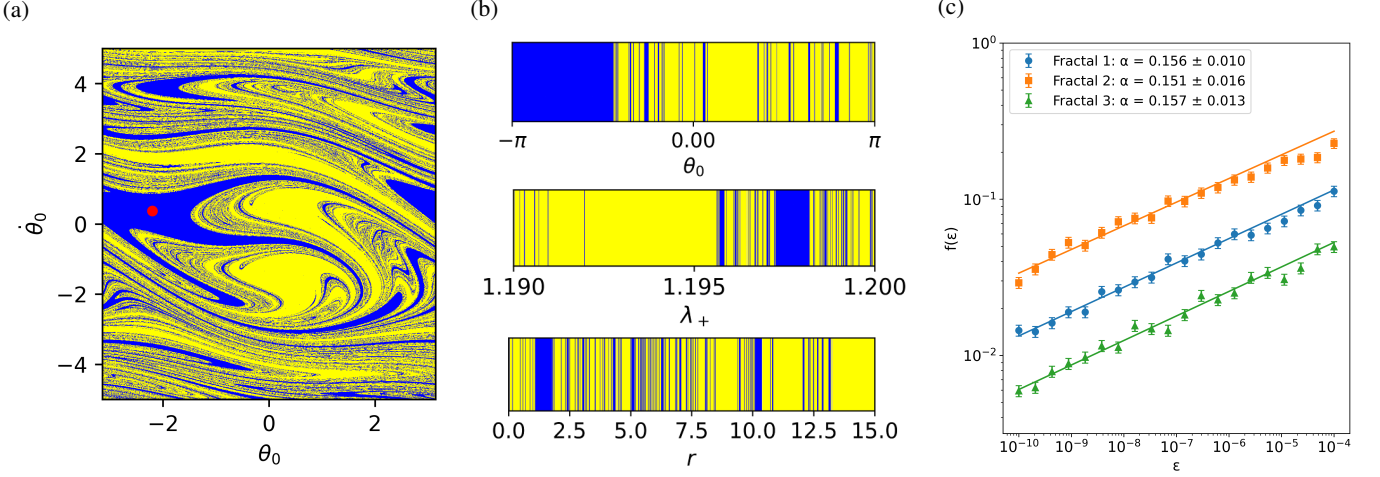


FIG. 7: The three fractals in the forced pendulum (13) have the same co-dimension α . (a) Phase space at the Poincaré surface of section showing the basin of attraction (in blue) of the fixed point $(\theta^*, \dot{\theta}^*) \approx (-2.20, 0.37)$ (red circle) for $\lambda = 1.195$. (b) Plot of the function $\phi(r, x_0; \Lambda(s))$ in Eq. (4) as a function of different variables, with blue corresponding to $\phi = \text{track}$ and yellow to $\phi = \text{tip}$. From top to bottom, the panels show the dependence of ϕ on the initial conditions $x_0 = (\theta, \dot{\theta} = 0)$ (with $r = \lambda_+ = 0$, Fractal 1), range of parameter variation λ_+ used in $\Lambda(s)$ (with $r \rightarrow \infty$, Fractal 2), and the rate of change r (with $\Delta\lambda = 1.195$, Fractal 3, $r_{c1} \approx 0.040$ and $r_{c2} \approx 13.246$). (b) Estimation of the fractal co-dimension α of the track/tip boundary for the three fractals shown in panel (b). We use the uncertainty algorithm^{12,18} and estimate α as the slope of the scaling between the fraction of ε -uncertain points $f(\varepsilon)$ and ε , see Appendix C for details.

boundary of the frozen system at the asymptotic parameter $\lambda = \lambda_+$. In this section, we provide a general theoretical explanation for these observations and discuss (sufficient) conditions for the appearance of fractals in R-tipping through the mechanism described below.

Our starting point is an autonomous dynamical system (1) which shows multistability and in which the attractor in focus (i.e., the fixed point x^*) at the parameter $\lambda = \lambda_+$ has a fractal basin boundary, i.e., a fractal boundary in the dependence of $\phi(x_0, r = 0; \Lambda(s) = \lambda_+)$ on the initial condition $x_0 \in \Omega \subseteq \mathbb{R}^d$. The existence of such fractal basin boundaries is well known in a variety of non-linear dynamical systems^{13,18,19}. In the typical transient chaos picture¹², the boundary is composed by the stable manifold W^S of the chaotic (hyperbolic) saddle that controls long-term transients. If the dimension of this manifold $D(W^S)$ satisfies $d - 1 < D(W^S) < d$, then W^S divides the d -dimensional phase space into regions that may converge to different attractors and therefore W^S may act as a fractal basin boundary¹⁹. We thus write:

Condition 1: the existence of a fractal saddle in the phase space $x \in \Omega \subseteq \mathbb{R}^d$ of F at $\lambda = \lambda_+$ with a stable manifold W^S with dimension $D(W^S)$ such that the co-dimension $\alpha(W^S) = d - D(W^S)$ is

$$0 < \alpha(W^S) < 1$$

and W^S acts as the boundary of the basin of attraction of the (fixed-point) attractor $x^*(\lambda_+)$.

The uncertainty exponent α_1 of Fractal 1 computed in the previous section (Sec. III) provides an estimation of the co-

dimension of the basin boundary and thus of the stable manifold of the fractal saddle, see Appendix C for details. Therefore, we have $\alpha(W^S) = \alpha_1$. The next two conditions ensure that this fractal object induces the appearance of fractals in the two natural settings of R-tipping, Fractals 2 and 3, involving the dependence of ϕ on $\Lambda(s)$ and r , respectively.

We first focus on the conditions for the existence of R-tipping. The dynamical system F at λ_+ is susceptible to rate-induced tipping if x^* and its basin of attraction are sensitive to changes in λ ⁹. In line with the sufficient conditions derived in Ref.⁷, we consider:

Condition 2: the parameter path $\Lambda(s)$ must be such that $x^*(\lambda_0)$ (i.e., the attractor at the starting parameter λ_0) is outside the basin of attraction of $x^*(\lambda_+)$ (i.e., the attractor at the final parameter λ_+).

More generally, a weaker condition that can still lead to tipping is to require x^* to leave the basin of attraction at least once in the path $\Lambda(s)$, i.e., there are s_a, s_b , with $s_a > s_b$, such that $x^*(\Lambda(s_a))$ is *not* in the basin of attraction of the attractor at s_b .

The last requirement for the appearance of fractals in R-tipping is to connect variations in parameters (e.g., λ_+, r) of the dynamics with variations in the trajectories in the phase space:

Condition 3: the autonomous dynamics F and parameter path $\Lambda(s)$ must be such that continuous variations in the parameter λ along $\Lambda(s)$ for

a fixed initial condition x_0 leads to a continuous curve in the phase space Ω for $n > 0$.

This last condition is satisfied in the examples above due to the continuity of $F(x; \lambda)$ and $\Lambda(s)$.

We now discuss how these conditions lead to the appearance of fractals in R-tipping. Condition 1 ensures that there is a fractal basin boundary in the phase space Ω (Fractal 1) at the asymptotic parameter $\lambda_+ = \lim_{s \rightarrow \infty} \Lambda(s)$.

For sufficiently small r , and stable path $\Lambda(s)$, $\phi(r, x_0; \Lambda(s)) = \text{track}$ because $x_0 = x^*(s_0)$ (i.e., initial condition in the attractor). Condition 2 ensures that $\phi(r \rightarrow \infty, x_0; \Lambda(s)) = \text{tip}$, and therefore, that there is at least one critical value r_c . For $r = r_c$, the trajectory $x(n)$ hesitates between tracking and tipping, approaching an edge state as $n \rightarrow \infty$. In this limit, $\lambda \rightarrow \lambda_+$ and thus the non-autonomous dynamics in Eq. (2) becomes effectively autonomous as in Eq. (1) with $\lambda = \lambda_+$. Thus, the edge state approached by the trajectory will typically be the chaotic saddle associated with Fractal 1²¹. Condition 3 ensures that small (continuous) variations in r or λ_+ around a boundary of $\phi(r, x_0; \Lambda(s))$ lead to slightly perturbed trajectories that create a curve in the phase space $\Omega \subseteq \mathbb{R}^d$. This curve expands exponentially in time n (due to the positive Lyapunov exponent of the saddle) so that for sufficiently large n it will generically intersect Fractal 1 (because its co-dimension is $0 < \alpha < 1$ as specified in Condition 1). These intersections lead to changes in the outcome of $\phi(r, x_0; \Lambda(s))$ at different critical values of λ_+ or r , leading to the appearance of Fractals 2 and 3 (respectively) with the *same* fractal co-dimension as Fractal 1:

$$\alpha_1 = \alpha_2 = \alpha_3. \quad (15)$$

The equality $\alpha_1 = \alpha_2$ between the fractals in the basin of attraction (Fractal 1) and in the (frozen) parameter space (Fractal 2) has been observed and discussed in Refs.^{18,22,23}.

In the argument above, we have neglected the dependence of α_1 on λ_+ . While a single λ_+ is used in Fractals 1 and 3 – and thus in the estimation of α_1 and α_3 –, Fractal 2 considers precisely the variation of ϕ on λ_+ . Therefore, the equality involving α_2 in Eq. (15) requires a point-wise estimation of α_2 , i.e., the pointwise-fractal dimension 2 around a critical value $\Delta\lambda_c = (\lambda_+ - \lambda_-)_c$ is equal to α_1 at λ_+ . In examples B and C, this motivated the use of small intervals of λ_+ around the value of interest (see Figs. 6a and 7a, middle panels). More generally, α_2 is dominated by the region of λ_+ with largest dimension (smallest α). The dimensions in Eq. (15) are computed for $\varepsilon \rightarrow 0$, which implies chaotic trajectories $n \rightarrow \infty$ and thus $\lambda \rightarrow \lambda_+$. For finite temporal and spatial scales ε , we expect the effective²⁴ fractal dimension $\alpha_2(\varepsilon)$ to follow $\alpha_1(\lambda(n))$.

V. DISCUSSION AND CONCLUSIONS

We have investigated a mechanism for the appearance of fractals in R-tipping. We have shown that if the attractor of a dynamical system F at parameter λ_+ has a basin of attraction with a fractal boundary, parameter changes that converge

to λ_+ have tracking-tipping transitions in an (uncountable) infinite number of critical rates r_c . Moreover, the set of such r_c 's have the same fractal co-dimension of the basin boundary. We provided general conditions for these results and illustrated them in three paradigmatic transiently-chaotic¹² systems subject to parameter changes as done in R-tipping settings^{1,7,25}. These results complement and share similarities to other interesting interplays between R-tipping and non-linear dynamics^{3–6,15,26}.

We have tested the validity of our results for different parameter-variation protocols $\Lambda(s)$. Still, all of them had a limiting case λ_+ . A more challenging case is whether our results can persist when no such limit is observed (e.g., when the parameter grow or decay continuously). This generalization requires considering the dimension of the pullback or snapshot saddle^{11,12}. One such scenario can be analyzed in our first example ($d = 1$ piecewise-linear map): a linear ramp $\Lambda(s) = s = rn$ leads to a single critical tipping rate r_c ; however, a fractal is still observed if the ramp is initially fast ($d\Lambda(rn)/dn > r_c$) but slows down ($d\Lambda(rn)/dn < r_c$) for large s . This example shows that fractals can also appear in R-tipping for more general parameter-changing protocols $\Lambda(s)$, provided that convergence to the moving attractor $x_n \rightarrow x^*$ is possible for large s .

Our analysis in simple dynamical systems intends to contribute to the understanding of generic rate-induced tipping phenomena. The ubiquity of fractal saddles and transient chaos in non-linear dynamics^{12,13} suggests that the fractals we observe can appear also in non-autonomous systems proposed as models of physical or biological systems. In fact, fractal edge states have been reported in climate models^{10,16,27} and our results predict the appearance of fractal R-tipping with the same co-dimension α as stated in Eq. (15). In these cases, our results can have practical consequence, such as quantifying (through α) the extreme sensitivity to small perturbations and extreme oscillations, as well as opportunities for intervention or control. We further expect that the full range of fractal phenomena present in transient chaos^{12–14} also appear in the R-tipping setting. For instance, we expect a fractal boundary separating three different asymptotic states (as in Fig. 5a) and the Wada property¹³ to appear in the dependence of ϕ on r .

ACKNOWLEDGMENTS

EGA thanks Hinke Osinga for helpful suggestions.

Appendix A: Complete expression of the modified tent map

A general expression for the extended tent map, as in Eqs. (6) and (7), valid for more general parameters is $x_{n+1} = F_A(x_n)$ with

$$F_A = \begin{cases} \mu \min(x_n - \lambda, 1 - (x_n - \lambda)) + \lambda, & x_n - \lambda < s_1, \\ a_1(x_n - \lambda) - b_1 + \lambda, & s_1 \leq x_n - \lambda < s_2, \\ a_2(x_n - \lambda) - b_2 + \lambda, & x_n - \lambda \geq s_2, \end{cases}$$

with $\lambda, \mu > 2, 0 < a_2 < 1$, and $1 < s_2 < 3\mu/4 - 1/2$ as free parameters. We fix the remaining parameters a_1, b_1, b_2 , and s_1 using the same constraints discussed in the main text after Eq. (6), i.e., setting the escaping region, re-injection region, and the attracting region of the intermediate regime to be the same in size. This leads to

$$a_1 = \frac{e_2}{e_2 - e_1}, \quad (\text{A1})$$

$$e_1 = 1 + \frac{1}{3}(s_2 - 1), \quad (\text{A2})$$

$$e_2 = 1 + \frac{2}{3}(s_2 - 1), \quad (\text{A3})$$

$$a_2 = \frac{1}{4}, \quad (\text{A4})$$

$$b_1 = a_1 s_1 - \mu(1 - s_1), \quad (\text{A5})$$

$$b_2 = b_1 + s_2(a_2 - a_1), \quad (\text{A6})$$

$$s_1 = \frac{a_1 e_1 + \mu}{a_1 + \mu}, \quad (\text{A7})$$

$$s_2 = \frac{\mu}{2}. \quad (\text{A8})$$

The case used in the main text – Eq. (6) and Fig. 1 – is retrieved choosing $a_2 = 1/4$, $\mu = 3$, $s_2 = \mu/2$, and $\lambda = 0$.

Appendix B: Tipping in the Hénon map with smooth boundaries

Figure 8 shows an example of a smooth (non-fractal) boundary of the tipping function ϕ in cases in which the attractor x^* at λ_+ has a smooth basin boundary.

Appendix C: Computation of the fractal dimension

The fractal dimension of the different sets of interest are computed using the uncertainty algorithm described in Refs.^{12,18} and implemented in our repository¹⁷. We begin by defining a one-dimensional line segment ($d = 1$) in the space of interest. In our case, this can be the phase space of initial conditions x_0 (Fractal 1), the parameter space λ (Fractal 2), or the rate space r (Fractal 3). Here we consider this line parametrized by y , with $y \in [y_a, y_b]$. We then compute the fractal co-dimension α with the following algorithm:

1. For a given scale $\varepsilon < |y_b - y_a|$, repeat the following steps until a pre-defined number M_u of uncertain points is obtained:
 - (a) Pick randomly with uniform probability a value $y \in [y_a + \varepsilon, y_b - \varepsilon]$ and neighbouring points $y_{\pm} = y \pm \varepsilon$.
 - (b) Iterate the dynamical system (2) for y and y_{\pm} and compute the value of the tipping function $\phi(y)$ and $\phi(y_{\pm})$.
 - (c) If $\phi(y) \neq \phi(y_{\pm})$, we consider y to be uncertain ($M_u \mapsto M_u + 1$).

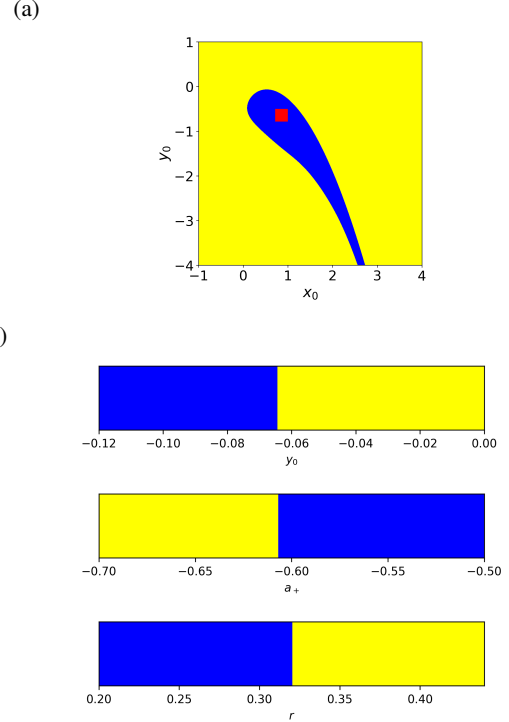


FIG. 8: Smooth basin boundary of the end fixed point yields smooth boundaries in the R-tipping region in the parameter space as well as in the rate space. (a) The basin of attraction boundary of the fixed point corresponding to $(a_+, b_+) = (-0.68, -0.75)$. Blue region indicates $\phi = \text{track}$, while yellow region indicates $\phi = \text{tip}$. (b) Plot of $\phi(r, x_0; \Lambda(s))$ in Eq. (4) – with blue corresponding to $\phi = \text{track}$ and yellow to $\phi = \text{tip}$ – as a function of different parameters (top to bottom): initial conditions $(x_0 = 0.5, y_0)$, corresponding to the basin-of-attraction of the fixed point for the end parameter $(a_+, b_+) = (-0.68, -0.75)$; the end parameter value $(a_+, b_+ = -0.75)$, for a fixed starting parameter $(a_0, b_0) = (0.20, 0.25)$; rate r using $(a_0, b_0) = (0.20, 0.25)$ and $(a_+, b_+) = (-0.68, -0.75)$ under parameter path Eq. (12).

2. Compute the fraction of uncertain points $f(\varepsilon) = M_u/M$, where M is the number of times the previous loop was performed (i.e., the number of tested points).
3. Reduce ε (e.g., $\varepsilon \mapsto \varepsilon/2$) and repeat the computation above.

The uncertainty exponent α is estimated as the scaling exponent between $f(\varepsilon)$ and ε . The fractal dimension D of the underlying set (i.e., the boundary between $\phi = \text{track}$ and $\phi = \text{tip}$ intersected transversely by y), in the limit of small ε , satisfies

$$D = 1 - \alpha.$$

We estimate α along a one-dimensional curve (a straight line) intersecting transversely the fractal set of interest, thus $0 \leq \alpha \leq 1$, and the uncertainty exponent α can be interpreted as the co-dimension of the fractal sets of interest.

The points shown in our numerical computations – Figs. 2, 6, and 7 – were estimated using $M_u = 1,000$ in Fig. 2 and $M_u = 150$ in Figs. 6 and 7. Error bars are computed assuming a negative binomial distribution. The slopes of the fitted lines correspond to the uncertainty exponent α and were estimated through linear regression. The associated 95% confidence intervals were obtained by repeating the fit after bootstrapping the points.

REFERENCES

- ¹P. Ashwin, S. Wieczorek, R. Vitolo, and P. Cox, “Tipping points in open systems: bifurcation, noise-induced and rate-dependent examples in the climate system,” *Philosophical Transactions of the Royal Society A: Mathematical, Physical and Engineering Sciences* **370**, 1166–1184 (2012), publisher: Royal Society.
- ²P. E. O’Keeffe and S. Wieczorek, “Tipping phenomena and points of no return in ecosystems: Beyond classical bifurcations,” *SIAM Journal on Applied Dynamical Systems* **19**, 2371–2402 (2020).
- ³J. Lohmann, D. Castellana, P. D. Ditlevsen, and H. A. Dijkstra, “Abrupt climate change as a rate-dependent cascading tipping point,” *Earth System Dynamics* **12**, 819–835 (2021).
- ⁴U. Feudel, “Rate-induced tipping in ecosystems and climate: the role of unstable states, basin boundaries and transient dynamics,” *Nonlinear Processes in Geophysics* **30**, 481–502 (2023).
- ⁵H. M. Alkhayuon and P. Ashwin, “Rate-induced tipping from periodic attractors: Partial tipping and connecting orbits,” *Chaos: An Interdisciplinary Journal of Nonlinear Science* **28**, 033608 (2018).
- ⁶B. Kaszás, U. Feudel, and T. Tél, “Tipping phenomena in typical dynamical systems subjected to parameter drift,” *Scientific Reports* **9**, 8654 (2019), publisher: Nature Publishing Group.
- ⁷C. Kiers, “Rate-Induced Tipping in Discrete-Time Dynamical Systems,” *SIAM Journal on Applied Dynamical Systems* **19**, 1200–1224 (2020), publisher: Society for Industrial and Applied Mathematics.
- ⁸S. Wieczorek, C. Xie, and P. Ashwin, “Rate-induced tipping: thresholds, edge states and connecting orbits,” *Nonlinearity* **36**, 3238 (2023), publisher: IOP Publishing.
- ⁹P. D. L. Ritchie, H. Alkhayuon, P. M. Cox, and S. Wieczorek, “Rate-induced tipping in natural and human systems,” *Earth System Dynamics* **14**, 669–683 (2023), publisher: Copernicus GmbH.
- ¹⁰J. Lohmann and V. Lucarini, “Melancholia states of the atlantic meridional overturning circulation,” *Phys. Rev. Fluids* **9**, 123801 (2024).
- ¹¹D. Jánosi and T. Tél, “Overview of the advances in understanding chaos in low-dimensional dynamical systems subjected to parameter drift: Parallel dynamical evolutions and “climate change” in simple systems,” *Physics Reports Overview of the advances in understanding chaos in low-dimensional dynamical systems subjected to parameter drift*, **1092**, 1–64 (2024).
- ¹²Y.-C. Lai and T. Tél, *Transient Chaos*, Applied Mathematical Sciences, Vol. 173 (Springer New York, New York, NY, 2011).
- ¹³J. Aguirre, “Fractal structures in nonlinear dynamics,” *Reviews of Modern Physics* **81**, 333–386 (2009).
- ¹⁴E. G. Altmann, J. S. E. Portela, and T. Tél, “Leaking chaotic systems,” *Reviews of Modern Physics* **85**, 869–918 (2013), publisher: American Physical Society.
- ¹⁵B. Kaszás, U. Feudel, and T. Tél, “Death and revival of chaos,” *Phys. Rev. E* **94**, 062221 (2016).
- ¹⁶V. Lucarini and T. Bódai, “Edge states in the climate system: exploring global instabilities and critical transitions,” *Nonlinearity* **30**, R32 (2017).
- ¹⁷J. Wang and Y. Zheng, “Fractal_tipping,” (2026), GitHub repository, https://github.com/wqc1105/Fractal_tipping.
- ¹⁸S. W. McDonald, C. Grebogi, E. Ott, and J. A. Yorke, “Fractal basin boundaries,” *Physica D: Nonlinear Phenomena* **17**, 125–153 (1985).
- ¹⁹C. Grebogi, E. Ott, and J. A. Yorke, “Basin boundary metamorphoses: Changes in accessible boundary orbits,” *Nuclear Physics B - Proceedings Supplements* **2**, 281–300 (1987).
- ²⁰In particular, taking $\lambda_- = \lambda_0$ allows us to check the track/tip condition for $r \rightarrow \infty$ in Fig. 5 for any two parameter pairs in Γ , even if the linear path in Eq. (12) leaves Γ leading to an unstable path for $r < \infty$.
- ²¹When the trajectory starts at $s \rightarrow -\infty$, this trajectory can be thought as the snapshot or pullback-attractor which is therefore at the stable manifold of a pullback saddle¹² that converges to the chaotic saddle as $n \rightarrow \infty$. When the limit $s \rightarrow -\infty$ is taken in such a way that $s = -rn$, with $n \in \mathbb{N}$, we ensure that the temporal evolution includes $s = 0$ and thus λ passes through $\lambda(s = 0)$ (as done in Ref.⁷); if, instead, we consider $s = s_0 - rn$ with arbitrary s_0 , we observed that there is no unique limit of ϕ as $s \rightarrow -\infty$, i.e., the sensitivity on the choice of s_0 persists, similar to the initial-condition dependence observed in partial tipping^{3,5}.
- ²²F. C. Moon, “Fractal boundary for chaos in a two-state mechanical oscillator,” *Phys. Rev. Lett.* **53**, 962–964 (1984).
- ²³Y.-C. Lai and R. L. Winslow, “Fractal basin boundaries in coupled map lattices,” *Phys. Rev. E* **50**, 3470–3473 (1994).
- ²⁴A. E. Motter, A. P. S. De Moura, C. Grebogi, and H. Kantz, “Effective dynamics in Hamiltonian systems with mixed phase space,” *Physical Review E* **71**, 036215 (2005).
- ²⁵Our definition of tracking in Eq. (4) considers only the asymptotic state, differently from other definitions⁴ which reserve tracking to trajectories that follow closely the frozen path of the attractor and use transient tipping⁷ or reversible tipping⁸ to describe trajectories that depart the vicinity of the frozen attractor but eventually settle in it. In our case, such departure takes place for the trajectories associated with the three fractals as they approach the fractal saddle at λ_+ . In our first example, $x^{u,3}$ separates these trajectories from the tracking trajectories that remain close to the attractor.
- ²⁶S. Panahi and Y.-C. Lai, “Global phase-space approach to rate-induced tipping: A brief review,” *Chaos: An Interdisciplinary Journal of Nonlinear Science* **35**, 043139 (2025).
- ²⁷J. Lohmann and P. D. Ditlevsen, “Risk of tipping the overturning circulation due to increasing rates of ice melt,” *Proceedings of the National Academy of Sciences* **118**, e2017989118 (2021), <https://www.pnas.org/doi/pdf/10.1073/pnas.2017989118>.